Int J Adv Manuf Technol (2006) 27: 645–654
DOI 10.1007/s00170-004-2242-0

ORIGINAL ARTICLE

Jing Shi · C. Richard Liu

On predicting chip morphology and phase transformation in hard machining

Received: 4 February 2004 / Accepted: 19 April 2004 / Published online: 9 March 2005

Abstract A finite element model is developed to predict the chip formation and phase transformation in orthogonal machining of hardened AISI 52100 steel (62HRC) using Polycristalline Cubic Boron Nitride (PCBN) tools. The model mainly includes a chip separation criterion based on critical equivalent plastic strain; a Coulomb's law for the friction at the tool/chip interface; a material constitutive relation of velocity-modified temperature; a thermal analysis incorporating the heat dissipated from inelastic deformation energy and friction; and an annealing effect model, in which the work hardening effect may be lost or re-accumulate depending on material temperature. This fully coupled thermal-mechanical finite element analysis accurately simulates the formation of segmental chips and predicts the phase transformation on the chips, as verified by experiment. It is found that high temperatures around the secondary shear zone causes fast re-austenitization and martensite transformation, while other parts of the chips retain the original tempered martensitic structure.

Keywords AISI 52100 steel · Chip morphology · Hard machining · Martensite · Phase transformation

1 Introduction

Hard machining has been established as a finishing process recently. It can produce comparable surface finish as abrasive superfinishing up to 0.4 μm in Ra [1]. This innovative process not only has great potential to save significant cost, to increase production flexibility, and to reduce the pollution due to dry cutting, but also yields parts with higher surface quality and longer service life [2]. The residual stresses in the parts produced by hard machining have less variance than those in ground parts [3]. Therefore, in rolling contact fatigue tests, hard turned parts have shown better fatigue performance and higher repeatability compared with ground parts [4]. On the other hand, hard-turned surfaces machined in different cutting conditions have exhibited very different fatigue performances up to 50 times in terms of number of cycles under the same loading condition. The discoveries motivate researchers to optimize cutting performance in terms of residual stresses and microstructure by optimizing cutting conditions for different applications.

There are a number of experimental works published regarding various research issues in hard machining [5–10]. We may measure residual stresses, cutting forces, chip morphology, and part distortion that current experimental techniques can achieve, but these techniques are not capable of studying many other issues, such as plastic stress and strain distribution during machining, or cutting temperature field and history. In contrast, the use of finite element (FE) modeling to analyze hard machining processes has some distinctive advantages, particularly in dealing with the issues that are beyond the capability of experimental techniques. Finite element modeling considers the fact that hard machining is a coupled thermal-mechanical process in which plenty of heat is generated, mechanical and thermal effects influence each other strongly, and work material properties change dramatically as the temperature changes. Also, it has to be able to simulate chip segmentation, because hard machining usually involves the formation of segmental chips. However, no existing publications have successfully simulated this process with solid experimental verification. This paper reflects the effort to construct a finite element analysis model to simulate the orthogonal cutting of hardened AISI 52100 steel and accurately predict chip formation, and to verify the proposed model extensively.

J. Shi (✉)
Department of Industrial & Manufacturing Engineering,
North Dakota State University,
Fargo, DN 58105, USA
E-mail: jing.shi@ndsu.edu
Tel.: +1-701-231-7119
Fax: +1-701-231-7195

C.R. Liu
School of Industrial Engineering,
Purdue University,
West Lafayette, IN 47907, USA

2 Background

Attempts to use numerical approaches to analyze the machining process have been paid more and more attention by researchers in recent years. A number of publications have been focused on the modeling of metal cutting processes. In the modeling of cutting soft metals, Akiyama [11] analyzed the thermal deformation of the cutting tool and the thermal stresses by using the finite element method. Lin [12, 13] developed a simplified orthogonal cutting model with the help of a shear plane, defined by chip geometry obtained experimentally, to study the effects of mechanical loads, thermal loads, and the degree of constraints on deformation stresses in machining. Shirakashi [14] used FEM to predict residual stress within the machined sublayer by orthogonal cutting, and the distortion of workpieces was calculated based on residual stress. Shih [15] proposed a 2D FEM model to simulate metal cutting based on the geometrical criterion of chip formation. Liu [16] investigated the effect of sequential cuts on residual stresses in a machined layer by cutting annealed stainless steel, and concluded that the residual stress can be controlled by optimizing the second cut. Shi [17] studied the effect of material constitutive models on the finite element analysis of the machining of HY-100 steel. Meanwhile, the finite element method has been proved an effective way to predict cutting temperature by adopting a moving heat source method together with kinematics, geometry, and energetic aspects of the metal cutting process [18, 19].

As for the numerical modeling of machining hard materials such as hardened steels or aerospace alloy materials, fewer publications could be found. Machining of hard materials often produces segmental chips. This is because the deformation is highly localized along the shear zone due to the low ductility of the materials and usually causes plastic instability, brittle to ductile transformation, and material failure at the surface where no hydrostatic pressure exists. Komanduri [20, 21] performed extensive experimental study on the chip segmentation of titanium alloys and alloy steels. It was found that the segmental chips are basically formed by catastrophic shear on the primary shear zone. The catastrophic shear occurs when the machining condition is favorable to the thermal concentration on a narrow band and the geometric constraint in the primary shear zone. Ueda [22] believed that, in addition to the catastrophic shear mechanism, segmental chips can also form only due to the ductile fracture from overstrain at the primary shear zone, and this mechanism applies to the machining of low carbon steels. Nakayama [23] showed that in machining hardened brass and hardened steels, the segmental chips were produced when the shear strain reached a critical value beyond what the workpiece material could withstand. Thus, one of the major criteria used to verify a proposed model for hard machining is whether the model could produce segmental chips and whether the produced chips from modeling resemble the actual ones. Other verification criteria include the comparison on cutting forces and temperature. Marusich [24] developed fracture criteria and a software code, AdvantEdge, to simulate orthogonal cutting with segmental chips in high-speed machining. Its failure criterion was based on the toughness of the work material and the critical crack distance. Sandstorm [25] used the same software code to model the orthogonal cutting of aluminum and titanium alloys. Ng [26] used the code FORGE2D to model the turning of hardened AISI H13 (28-49HRC), in which continuous chips were obtained. He also [27] used ABAQUS/Explicit v5.8 to simulate the segmental chip formation in the machining of the same material. However, it was actually found that a substantial morphology difference existed between the predicted and actual chips. Guo [28] modeled 3D hard machining of AISI 52100 steel and predicted the temperature of the tool-chip interface using ABAQUS/Explicit v5.8. The prediction error was less than 15% compared with the experiment result of Ueda [29] under the same cutting conditions. However, the fact that his 3D finite element model only produced continuous chips indicates that further improvement is needed.

3 Finite element modeling

In this study, the fully coupled thermal-stress analysis function in ABAQUS/Explicit v6.2 was adopted to analyze the orthogonal machining of hardened AISI 52100 steel. The explicit method was used mainly because it has the advantages of computational efficiency for highly nonlinear problems such as most manufacturing processes, and it is very suitable for modeling brief and transient dynamic events [30]. Due to the simple geometrical configuration of orthogonal cutting, all initial meshes were directly generated in the ABAQUS input file, and the post processing work was performed using ABAQUS Viewer. All of the computation work was carried out on a SUN SPARC 4-CPU workstation.

3.1 Initial mesh

Two cutting conditions were selected for finite element modeling. Both conditions have a depth of cut of 0.1 mm, a cutting speed of 3.03 m/s, and a clearance angle of 5°. However, two rake angles, i.e., $-5°$ and $-25°$ for conditions 1 and 2 respectively, were chosen to ensure the validity of the proposed model and investigate the effect of rake angle on cutting performance. Both geometrical models include 7500 four-node solid elements and 7826 nodes. In addition, section controls were used to prevent the potential distortion of elements from large initial impacts.

3.2 Material properties

The work material was assumed to be thermal elastic-plastic. The material elasticity needs to be considered because the high ratio of hardness versus Young's modulus induces an appreciable amount of local elastic recovery after the tool passes through [23]. Shi [31] obtained the flow stress data of hardened AISI 52100 steel at a constant strain rate and excluded the temporal tempering effect on flow stress. These data, as shown in Table 1, were utilized in the model by adding the effect of

Table 1. Engineering strain and stress at elevated temperature for hardened AISI 52100 steel

Temperature (°C)	20	200	400	600	800
Yield stress (MPa)	1394.3	1160.8	908.3	413.7	302.8
Tensile strength (MPa)	1738.7*	2151.1	1551.2	934.4	310.5
Yield strain (%)	0.63	0.81	0.66	0.41	0.35
Necking strain (%)	0.96*	1.97	1.56	1.45	1.02
Young's modulus (GPa)	208.14	163.33	154.32	112.8	103.4

* The tensile strength and necking strain at room temperature are in fact the fracture stress and strain since the workpiece fractured before necking could occur.

high strain rate in machining. One famous relationship between strain rate and temperature was adopted. First derived from the well-known Zener and Holloman equation [32], the relationship between strain rate and temperature may be expressed as

$$Z = \dot{\varepsilon}_p \cdot \exp(U/KT)\,, \tag{1}$$

where $\dot{\varepsilon}_p$ is the plastic strain rate, T is the absolute temperature, U is an activation energy, and K and Z are constants at a given stress and strain. Based on the above equation, MacGregor and Fisher [33] developed the concept of velocity-modified temperature, T_v, in the formulation of

$$T_V = T\left(1 - A\ln\left(\dot{\varepsilon}_p/\dot{\varepsilon}_0\right)\right), \tag{2}$$

where A and $\dot{\varepsilon}_0$ are constants related to the activation process for plastic flow, and take the value of 0.09 and 1.0, respectively, according to Oxley [34]. This equation shows that the flow stress is a unique function of T_v at a given strain level.

3.3 Chip separation

There are two commonly used criteria – namely, a geometrical criterion and an equivalent plastic strain criterion – to separate the chip from the machined surface in finite element analysis. Many works have adopted the former separation criterion [16, 26]. It is convenient to use but its physical meaning is very difficult to explain. Therefore, the latter criterion was adopted in this study. In fact, it has become popular and effective in modeling chip separation of metal cutting [15, 35]. According to this criterion, the material fails when the equivalent plastic strain reaches a critical value. This corresponds to the shear failure mode defined in ABAQUS, which implies that the physical shear failure occurs when the damage parameter ϖ reaches unity:

$$\varpi = \sum\left(\frac{\Delta\bar{\varepsilon}^{pl}}{\bar{\varepsilon}_f^{pl}}\right), \tag{3}$$

where $\bar{\varepsilon}_f^{pl}$ is the critical equivalent plastic strain. This value does not change with cutting conditions in hard machining according to Nakayama [23]. In orthogonal machining of hardened bearing steels, it was found that the formation of the segmental chip is quite different from the continuous chip formation based on traditional shear angle theories. In spite of the change of rake angle, the inclination angle of segmentation was found to be almost constant. The relation between the segmentation angle ϕ_c and critical shear strain γ_c is as follows:

$$\phi_c = \frac{\pi}{4} - \frac{\gamma_c}{2}\,. \tag{4}$$

3.4 Friction

Coulomb's friction law was applied to the sticking and sliding frictions along the tool/chip interface. Whether the friction is sticking or sliding on the interface depends upon the normal stress acting on the interface. The formulation could be expressed as follows:

$$\begin{aligned} &\tau = \mu p \quad \text{when } \tau < \bar{\tau}_{\max}, \\ &\tau = \bar{\tau}_{\max} \quad \text{when } \tau \geqslant \bar{\tau}_{\max}\,, \end{aligned} \tag{5}$$

where $\bar{\tau}_{\max}$ is maximum equivalent shear stress, μ is the average friction coefficient, and p is the friction stress along the interface. The formulation indicates that the friction is sliding when the friction stress is below $\bar{\tau}_{\max}$, and it becomes sticking when the friction stress is equal to or larger than the $\bar{\tau}_{\max}$ regardless of the contact normal stress.

The estimation of μ along the tool/chip interface for each cutting condition is based on the experimental measurement of cutting force during orthogonal cutting,

$$\mu = \frac{F_f\cos\alpha + F_t\sin\alpha}{F_t\cos\alpha - F_f\sin\alpha}, \tag{6}$$

where F_t and F_f are the measured forces in the tangential and feed directions, respectively, α is the rake angle. The measured F_t and F_f, as well as the calculated friction coefficient μ, for both cutting conditions, are shown in Table 2. In addition, the commonly accepted estimation of $\bar{\tau}_{\max}$ is expressed as

$$\bar{\tau}_{\max} = \sigma_y/\sqrt{3}\,, \tag{7}$$

where σ_y is the uni-axial yield flow stress of the work material.

3.5 Generated heat

The heating of material during machining may cause thermal damage to the machined surfaces and significantly affect the temperature-dependent material properties. In general, the generated heat during machining processes can be classified into friction heat along the tool/chip interface, heat due to inelastic energy dissipation, and latent heat. In this study,

Table 2. Calculated initial friction coefficient along the tool/chip interface

Cutting condition	Rake angle	Tangential force (N/mm)	Feed force (N/mm)	Initial friction coefficient
1	−5°	284.21	158.95	0.46
2	−25°	326.8	347.3	0.36

we only considered the first two sources and neglected the last one.

For inelastic energy dissipation as a heat source, plastic straining results in a heat flux per unit volume of

$$r^{pl} = \eta\sigma \cdot \dot{\varepsilon}^{pl} , \tag{8}$$

where r^{pl} is the heat flux, η is a factor indicating the portion of inelastic mechanical energy dissipated into heat (0.9 by default in this study), and $\dot{\varepsilon}^{pl}$ is the rate of plastic straining.

The rate of frictional energy dissipation as a heat source is given by

$$P_{fr} = \tau \cdot \dot{\gamma} , \tag{9}$$

where τ is the friction stress, and $\dot{\gamma}$ is the slip rate. Thus, on each contacting surface, the amount of heat flux is assumed to be

$$q = 0.5\eta P_{fr} . \tag{10}$$

Latent heat should only be taken into account when solidification and/or fluidification occur in a manufacturing process. In the machining of hardened steels, the material may experience dynamic recrystallization and recovery or even martensite transformation, and in turn, the molecular mobility may generate a very small amount of latent heat. Nevertheless, the change of phase is normally limited to the solid state, so the breaking or forming of intermolecular bonds is far less significant than fluidification, sublimation, etc. As a result, it is reasonable to assume the generated latent heat in hard machining is negligible.

3.6 Annealing effect

In a thermal-mechanical process, the material point will lose its hardening memory when the material temperature increases to a critical value. The equivalent strain is reset to zero to remove the prior work-hardening history. This is called the annealing effect. The material work-hardens again if its temperature drops below the critical value in the subsequent steps. Therefore, it is possible that the material accumulates and loses the work hardening effect many times as long as the temperature exceeds and goes back below the critical value again and again. We took this effect into consideration by setting a critical temperature for the work material.

Although static annealing at low temperature could fully eliminate the entangling of dislocations and work hardening history, the critical temperature in a high-speed machining process should be higher because of the extremely short duration. This value for a metal material is assumed to be the point in between the start of austenitization (temperature A_1) and the completion of austenitization (temperature A_3). The average of A_1 and A_3 is taken to be the critical temperature. AISI 52100 steel mainly consists of about 1% C, 1.6% Cr and Fe for the rest. Based on the C-Fe-Cr phase diagram, at C = 1% and Cr = 1.6% [36], this temperature is about 850 °C.

4 Experiment

The raw materials are cold-rolled and annealed AISI 52100 steel tubes with a 7.62 cm inner diameter and an 8.0 cm outer diameter for the purpose of conducting orthogonal machining. The chemical composition of the material is shown in Table 3. The raw materials went through the following industrial heat treatment procedure to obtain uniform hardness (62HRC) and microstructure. The parts were held at 843 °C in 1% carbon potential atmosphere, and thereafter, they were quenched in oil and kept at 60 °C. A sub-zero treatment resulting in the significant reduction of retained austenite was performed to improve the stability of the work material. The parts were tempered at 150 °C to reduce brittleness and stress concentration while increasing ductility and toughness, and then they were cooled down to room temperature.

The set-up schematic of the orthogonal hard machining experiments is shown in Fig. 1, with the detailed machining pa-

Table 3. Chemical composition of AISI 52100 steel

Specification	C (%)	Mn (%)	P (%)	S (%)	Si (%)	Cr (%)
AISI 52100	0.98 ~ 1.1	0.25 ~ 0.45	0.025	0.025	0.15 ~ 0.3	1.3 ~ 1.6

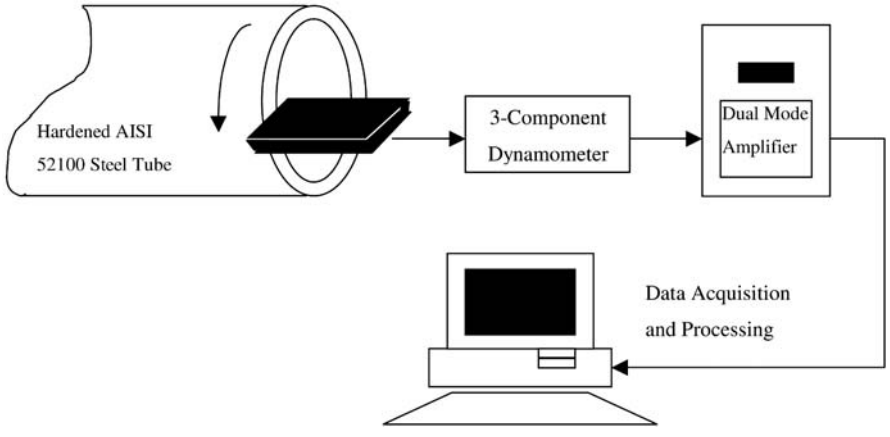

Fig. 1. Set-up schematic of orthogonal machining of hardened AISI 52 100 steel

Table 4. Machine set-up and cutting parameters

Workpiece	AISI hardened steel tube with 8 cm OD and 7.62 cm ID
Cutting tool geometry	BGNG-422, BGNG-422-0820 (20° T-land preparation)
Cutting tool materials	BZN8100 (by GE superabrasive)
Rake angle	−5° (BGNG-422), −25° (BGNG-422-0820)
Machine	Fryer CNC lathe
Coolant	None
Chucking	Standard 3-jaw
Cutting speed	3.03 m/s
Depth of cut	0.1 mm
Dynamometer	3-component Kistler dynamometer

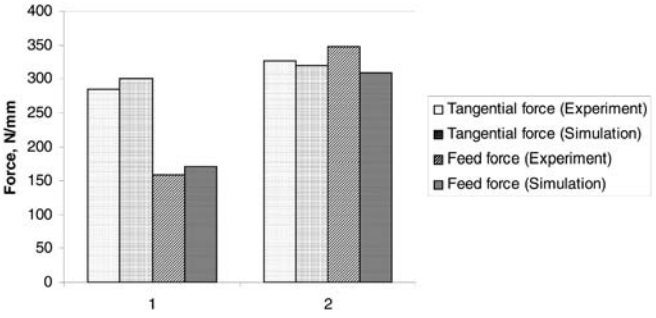

Fig. 2. Force comparison between simulation and experiment for cutting conditions 1 and 2

rameters shown in Table 4. A Fryer CNC lathe was used to conduct the machining. A customized tool holder was used with BGNG-422 cutting inserts to define a rake angle of −5° and clearance angle of 5°, and with BGNG-422-820 inserts to define a rake angle of −25° due to their honed 20° T-land. The cutting inserts from GE Superabrasive are made of BZN8100 PCBN (70%CBN + 30%TiN). The edge radius of the inserts is negligibly small so that they can be considered as perfectly sharp. A fixed rotation rate of 788.8 rpm was used, and, as a result, a cutting speed of 3.03 m/s was achieved. The feed used was 0.1 mm/revolution to achieve the desired depth of cut. The cutting forces were measured by a Kistler three-component dynamometer. Machined chips were collected for further observation and metallurgical examination.

To obtain the chip morphology and identify their microstructure, the chips were mounted in bakelite. The mounted samples were polished carefully with enough water as coolant to avoid extra strain hardening effects or thermal effects for a micro-hardness measurement. Only when no scratches could be seen under an optical microscope at a magnification of 400 was the morphology of the chips observed and measured. The microstructure of the chips was observed under an optical microscope and a JEOL 35CF scanning electron microscope after etching with a 2% nital solution. The microhardness was measured to help further identify phase transformation by performing a Knoop hardness test on a Leco hardness indenter. To ensure measurement quality, a very small indentation load of 10 g was used, four to six readings were taken at the same depth, and the average value was used.

5 Results and discussion

5.1 Cutting force comparison

As mentioned earlier, two cutting conditions with different rake angles were simulated and compared with experiment. Other cutting parameters are kept the same for the two conditions. Figure 2 shows the comparison between predicted and measured cutting forces. On the whole, the predicted forces do not deviate from the measured forces more than 15%. For condition 1 under a −5° rake angle, the measurement readings are 158.95 N/mm in feed force and 284.21 N/mm in tangential force, while the predictions are 170.4 N/mm and 300.1 N/mm respectively. When the rake angle is −25°, the measurement shows 347.3 N/mm in feed force and 326.8 N/mm in tangential force, while the predictions are 320.2 N/mm and 308.4 N/mm respectively. Both the measurement and prediction show that the tangential force is larger than the feed force under a −5° rake angle, while this trend is reversed under a −25° rake angle. The same phenomenon was also reported and confirmed in the literature [7, 23]. In addition, one unique characteristic of hard machining is that the feed force (or the thrust component in 3D cases) may become much larger than other force components with the existence of large flank wear [8, 23, 37]. Nevertheless, it cannot be observed in this study because a fresh sharp edge for each cut was used in experiment and no flank wear effect was included.

5.2 Chip morphology

We obtained segmental chips from both finite element simulation and actual machining experiments. Figures 3 and 4 show the formed chips from actual cutting under cutting conditions 1

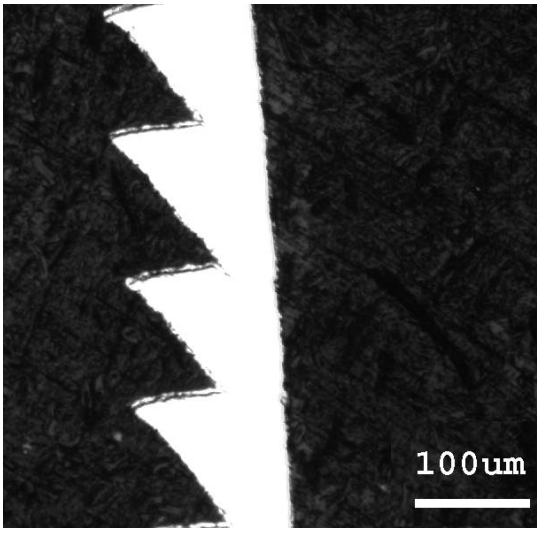

Fig. 3. Morphology of a formed chip under cutting condition 1

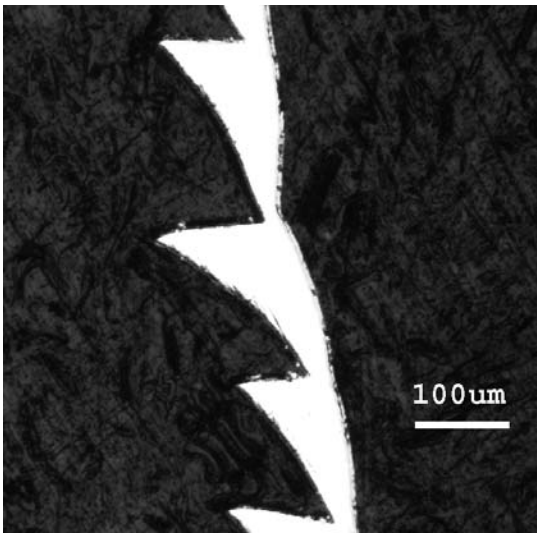

Fig. 4. Morphology of a formed chip under cutting condition 2

and 2, respectively. Meanwhile, Figs. 5 and 6 show the morphology of predicted chips for cutting conditions 1 and 2, respectively. The dimensions of the actual chips in bakelite were measured on an optical microscope, while the dimensions of the simulated chips were computed from the coordinates of the deformed elements. It can be seen that, for both conditions, the morphology and dimensions of the simulated chips are in very good agreement with those of actually formed chips. Take cutting condition 1 as an example, the average maximum height of the teeth on the actual chip is 0.145 mm while that of the teeth on the simulated chip is 0.153 mm. In the meantime, the average interval between teeth on the actual chip is 0.1376 mm, and, by comparison, the average interval between teeth on the simulated chip is 0.140 mm. In addition, the simulation shows that tooth intervals become larger and the tooth tails are more stretched under a larger negative rake angle, which is also verified by the actual chip as shown in Fig. 4. The average actual tooth interval changes from 0.1376 mm to 0.181 mm as the rake angle changes from $-5°$ to $-25°$, while the average simulated tooth interval changes from 0.140 mm to 0.1857 mm with a change of rake angle. A longer tooth tail indicates that the material in the area is under more severe plastic deformation and more heat is generated.

Based on the chip morphologies, the shear angles in simulation and actual machining for both conditions were calculated. The shear angles, for cutting condition 1, are 45.1° and 46.5° for simulation and actual cutting, respectively, while, for cutting condition 2, they are 41.1° and 43.9°, respectively. This result supports the finding that shear angle does not change much with the change of rake angle in actual hard machining, as was discovered by Nakayama [23].

5.3 Temperature distribution on the formed chips

The plastic stress and strain in the hard machining simulation are highly localized along the primary shear zone according

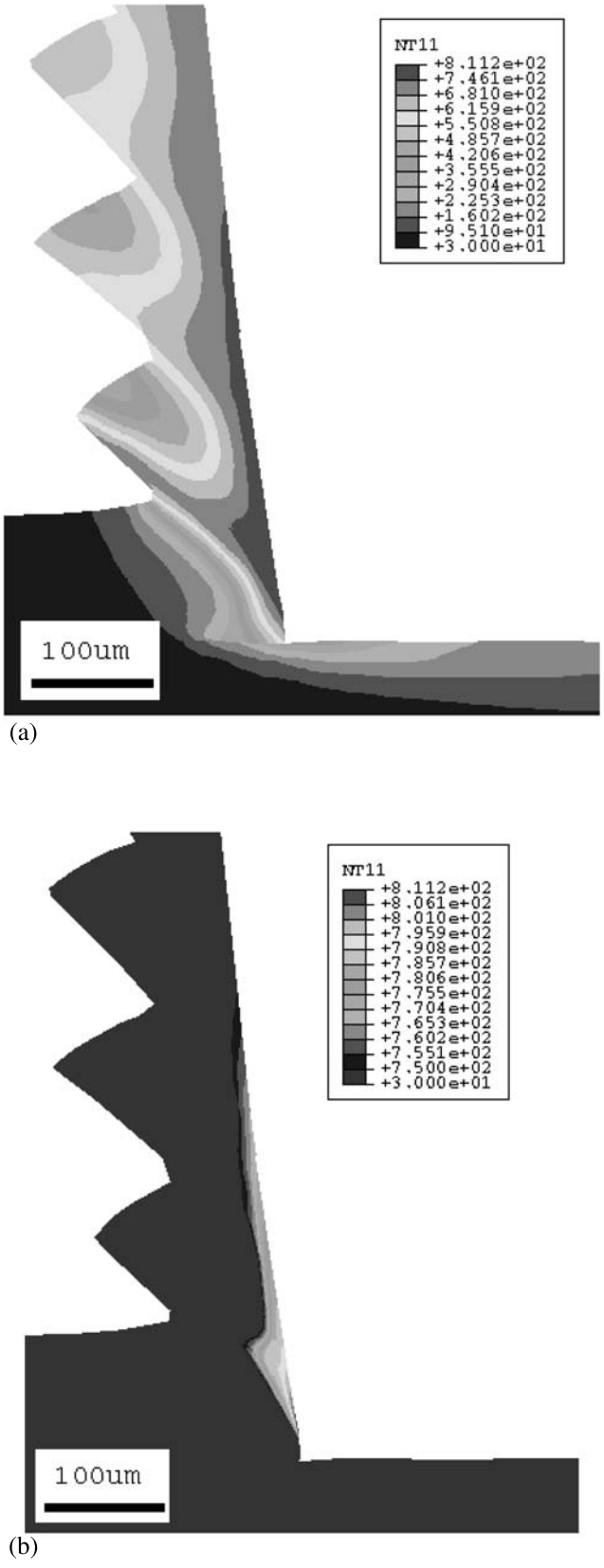

Fig. 5. a Temperature distribution on the simulated chip under cutting condition 1. **b** Isolated high-temperature area under cutting condition 1

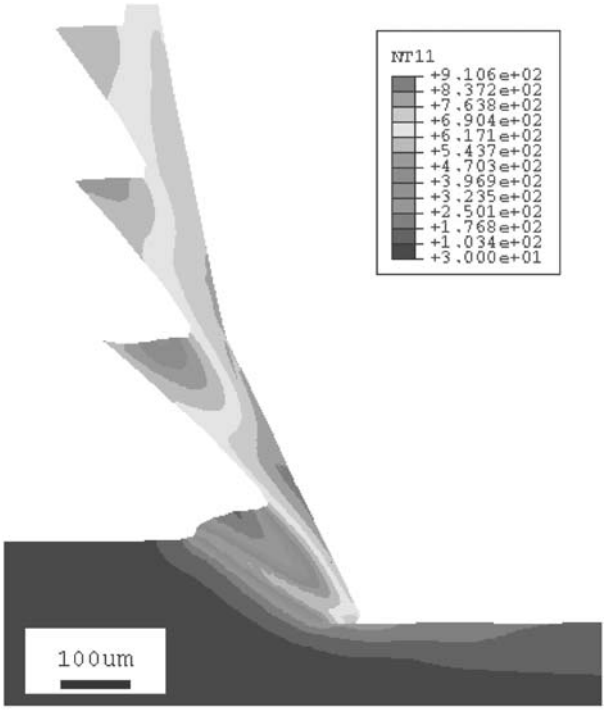

(a)

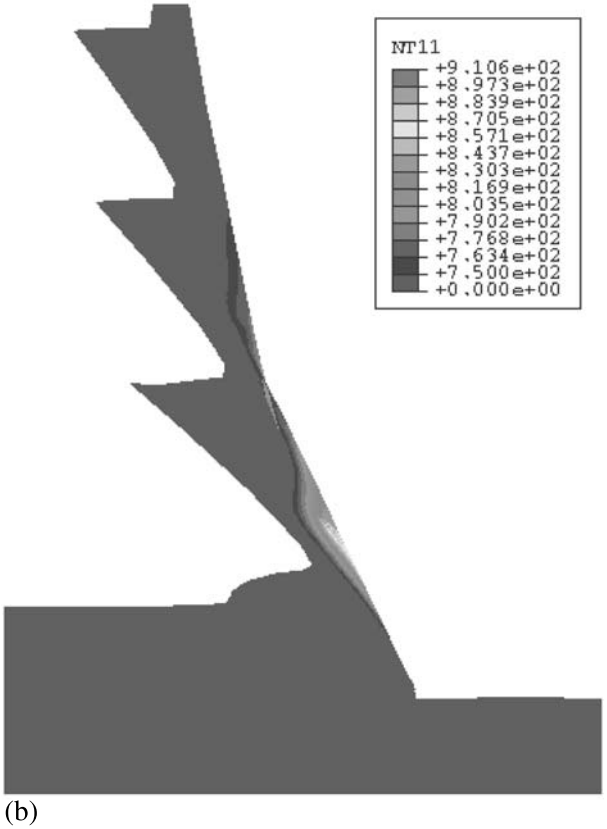

(b)

Fig. 6. a Temperature distribution on the simulated chip under cutting condition 2. **b** Isolated high-temperature area under cutting condition 2

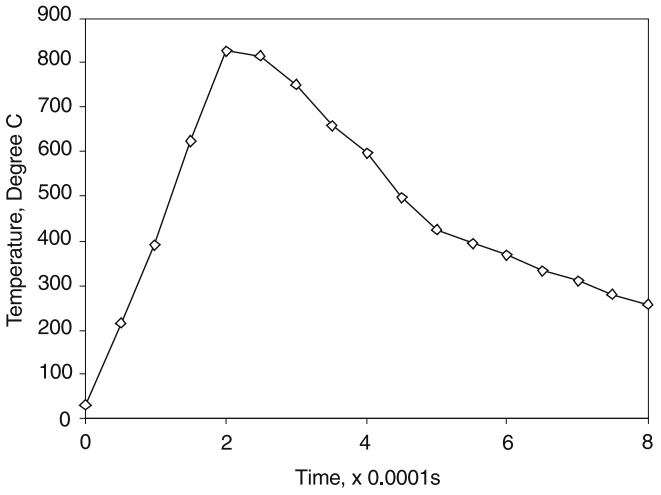

Fig. 7. Temperature history of a material point in the high-temperature area under cutting condition 2

to our observation, and the resultant temperature distributions under cutting conditions 1 and 2 are shown in Figs. 5a and 6a, respectively. It can be seen from both figures that the temperature of a narrow band in the primary shear zone is much higher than its surroundings, and chip segmentation takes place along this band. This observation is consistent with the catastrophic shear mechanism, which involves two major steps according to Komanduri [20, 21]. The first step is the occurrence of strain localization and heat concentration due to plastic instability, while the second step is the flattening of the heated half wedge by the advancement of the tool. In fact, the chip formation in Fig. 6a is the first step of this mechanism, while Fig. 5a clearly shows the second step. In the meantime, it is noted that the maximum temperature on the chip is higher than 750 °C for both cutting conditions, so high-temperature (greater than 750 °C) areas are isolated from other areas, as shown in Figs. 5b and 6b. Obviously, the high-temperature areas are mainly along the tool-chip interface for both cases. This is the result of the accumulative energy dissipation of the friction along the tool-chip interface and the inelastic deformation in the secondary shear zone. Moreover, it can be seen that the high temperature areas are mostly concentrated in the "tail" of each segmental chip tooth because of the severer plastic deformation at these positions. The temperature history of a typical point in high-temperature area is shown in Fig. 7. It could be seen that the heating speed is larger than 4×10^6 °C/s, while the average cooling speed is about 1×10^6 °C/s in the range of 800 °C down to 600 °C, and 7.5×10^5 °C/s in the range of 600 °C down to 300 °C. The following question naturally arises: can phase transformation take place in these high-temperature areas?

5.4 Phase transformation on the formed chips

Phase transformation here refers to re-austenitization from the original structure – tempered martensite for this material, and the re-formation of untempered martensite from austenite due to

rapid cooling. On one hand, we found that the austenitization temperature for this material is about 750 °C in a heat treatment experiment, so the high-temperature regimes on the simulated chips in Figs. 5b and 6b have the potential of re-austenitization. On the other hand, the normal austenitization process, involving the diffusion of C atoms, takes a certain amount of time to reach uniformity. The extremely short heating time (less than 10^{-3} s) and very high heating rate (greater than 10^5 °C/s) in hard machining do not allow enough time for C atoms to diffuse throughout the austenite structure. This means that the phase transformation in a hard machining process, if it occurs, involves the formation of the austenite with little dissolving of carbide and diffusion of C atoms. Indeed, Orlich [38] observed that the transformation from martensite to austenite is finished with no diffusion and no evidence of the increase of phase transformation temperature due to rapid heating was found. Also, Tonshoff [8] studied the changes of chemical composition of ASTM 5115 steel (60HRC) in hard machined surfaces with a white layer. Using discharge optical emission spectrometry, an even concentration of all elements (Mn, Cr, C, Si, and S) was detected, and it was independent of the depth. In other words, no element concentration transition from the white layer to the over-tempered layer was found. In addition, it is well-known that martensite forms when the austenitization is followed by rapid cooling, at a rate of larger than 10 °C/s for AISI 52100 steel based on its CCT diagram [39]. The formation of martensite is not related to carbon diffusion; instead, it involves the cooperative coordinate shift of an atom that happens in approximately 0.1 μs [40]. Thus, we believe that the material in the isolated high-temperature areas during hard machining can be re-austenitized and then transformed into untempered martensite because their peak temperature is higher than the austenitization temperature and the subsequent cooling rate is much higher than 10 °C/s.

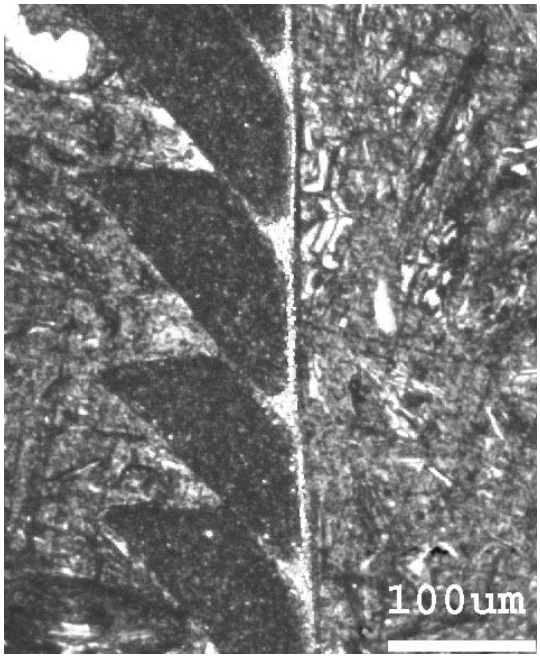

Fig. 8. Etched chip for cutting condition 1

Fig. 9. Etched chip for cutting condition 2

The examination of etched chip samples supports our speculation. As shown in Figs. 8 and 9, the segmental chips after etching had two distinctive areas visible under optical microscopy. One was the dark area, while the other was a white shiny layer that was very difficult to etch. It is commonly believed that the dark area consists of a microstructure similar to bulk material, while the white area is mainly freshly formed martensite with little tempering. To prove this, a hardness test on the dark area and white layer was conducted. Figure 10 shows that, for cutting condition 1, the average hardness of the white layer material is 832.7 kg/mm^2, while that of the dark area is 785.8 kg/mm^2; for cutting condition 2, the average of the white

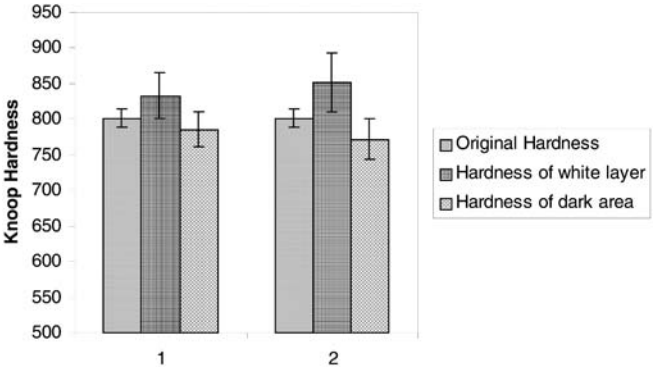

Fig. 10. Hardness comparison between the original material, white layer, and dark area in the chip for both cutting conditions

layer material is 851.6 kg/mm^2, while that of the dark area is 772 kg/mm^2. Also, the original bulk material has a Knoop hardness of 801.1 kg/mm^2. Thus, the hardness of the white layer area is significantly higher than the original bulk material and the material in dark area on the chip cross-section. Figure 11 shows the Knoop indentations on the chip produced under cutting condition 2, and it is clear that the tail of the chip tooth is harder than other regimes. Combining the temperature distributions in Figs. 5 and 6 and the temperature history in Fig. 7, we confirm that phase transformations – namely, re-austenitization and austenite-martensite transformations – took place in the white layer areas on the formed chips. Furthermore, Figs. 8 and 9 also show that the white layer areas concentrate in the tails of each chip tooth, which agrees with the simulation result in Figs. 5 and 6. If the white layer areas are carefully compared with the simulated high-temperature areas (above 750 °C), it is not difficult to find that the simulation and metallurgical observation match each other very well in size and shape for both cutting conditions. In addition, it can be seen that the white layer of cutting condition 2 is harder than that of cutting condition 1. We believe that the higher temperature under condition 2 plays a key role here. A higher temperature provides higher thermal activation energy, and therefore dissolves more carbides and releases more carbon atoms even though no diffusion is involved. Thus, after rapid cooling, the structure of untempered martensite is more distorted, resulting in a higher hardness.

The SEM observations of the bulk material and the dark area of the etched chip, as shown in Fig. 12, further reveal that the dark area material has a very similar tempered martensitic structure as the bulk material. It can be seen that, except the white layer, other materials in the machined chips did not experience phase transformation during hard machining because of a low cutting temperature. On the other hand, due to the extremely short heating history, the material softening effect in the dark areas is not significant either, as shown by the hardness comparison in Fig. 11.

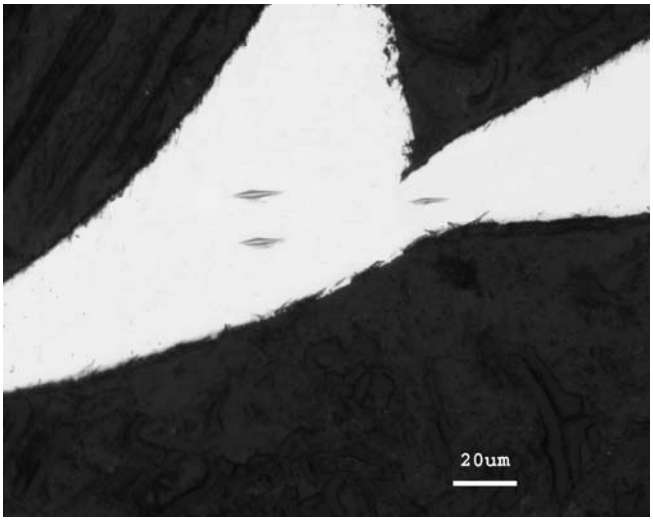

Fig. 11. Knoop indentations on the chip produced by cutting condition 2

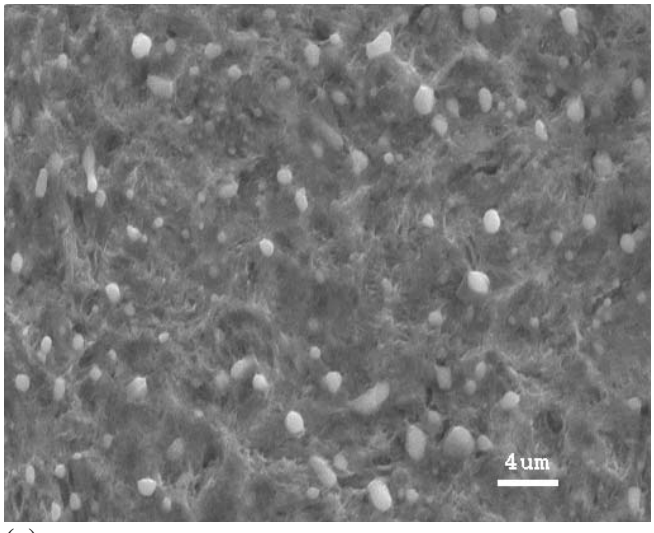

(a)

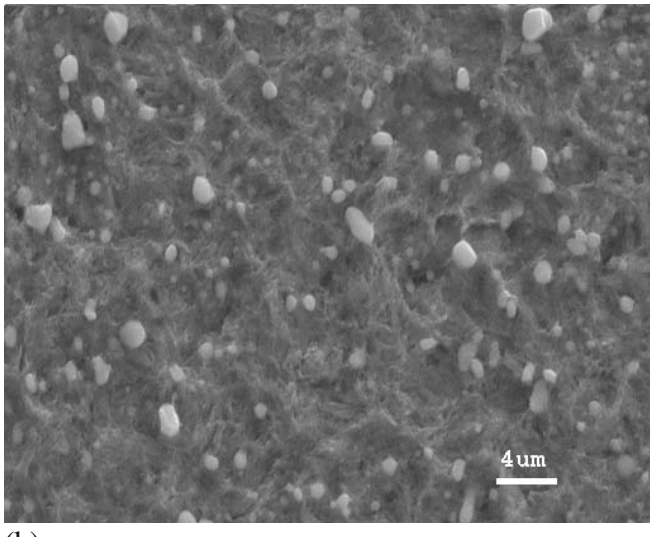

(b)

Fig. 12a,b. SEM micrographs of **a** the structure of the original bulk material and **b** the structure of the material from the dark area on the chips

6 Conclusions

We have considered the thermal-mechanical coupling nature of machining, developed an FE model to simulate the orthogonal hard machining, and verified the model experimentally by comparing cutting forces and chip morphologies, conducting a material hardness test and microstructure observation. In summary, the following conclusive remarks could be made:

1. Compared with experiment, the finite element model is capable of predicting the cutting forces in orthogonal machining of hardened AISI 52100 steel with less than a 15% error.
2. Segmental chips can be simulated by the proposed model, and their morphology and dimensions are consistent with those of the chips obtained from actual machining.

3. The areas in the simulated chip with high cutting temperature for phase transformation match the white layer areas on the actual chips. It proves that fast re-austenitization and martensite transformation can take place in hard machining. More importantly, the prediction of phase transformations further verifies the proposed finite element model.

Acknowledgement The support of National Science Foundation award 9713748-DMI is gratefully acknowledged.

References

1. Liu CR, Mittal S (1995) Single step super-finishing resulting in superior surface integrity. J Manuf Syst14:124–133
2. Liu CR, Mittal S (1996) Single step super-finish hard machining: feasibility and feasible cutting conditions. Robot Comput Int Manuf Syst 12(1):15–24
3. Liu CR, Yang X (2001) The scatter of residual stresses due to machining and grinding. J Mach Sci Technol 5(1):1–22
4. Agha S, Liu CR (2000) Experimental study on the performance of superfinish hard turned surfaces in rolling contact. Wear 244:52–59
5. Matsumoto Y (1986) Effect of hardness on the surface integrity of AISI 4340 steel. J Eng Ind 108(3):169–175
6. Konig W. (1993) Turning versus grinding – a comparison of surface integrity aspects and attainable accuracies. Ann CIRP 42(1):39–43
7. Abrao AM, Aspinwall DK (1996) The surface integrity of turned and ground hardened bearing steel. Wear 196:279–284
8. Tonshoff HK, Wobker HG, Brandt D (1995) Hard turning – influences on the workpiece properties. Trans NAMRI/SME 23:215–220
9. Barbacki A, Kawalec M (1997) Structural alterations in the surface layer during hard machining. J Mater Process Technol 64:33–39
10. Wang JY, Liu CR (1999) The effect of tool flank wear on the heat transfer thermal damage and cutting mechanics in finish hard turning. Ann CIRP 48(1):53–58
11. Akiyama T (1977) Thermal deformation analysis of cutting tools by the finite element method. Bull Japan Soc Precis Eng 11(3):139–128
12. Lin ZC, Pan WC (1993) A thermoelastic-plastic large deformation model for orthogonal cutting with tool flank wear-part I: computational procedures. Int J Mech Sci 35(9):829–840
13. Lin ZC, Pan WC (1993) A thermoelastic-plastic large deformation model for orthogonal cutting with tool flank wear-part II: machining application. Int J Mech Sci 35(9):841–850
14. Shirakashi T (1994) The analytical prediction of residual stress within machined sublayer and its effect on accuracy. Int J Japan Soc Precis Eng 28(3):200–205
15. Shih AJ (1995) Finite element simulation of orthogonal metal cutting. J Eng Ind 11: 84–93
16. Liu CR, Guo YB (2000) FEM analysis of residual stresses on the sequential machined surface. J Mech Sci 42:1069–1089
17. Shi J, Liu CR (2004) The influence of material models on finite element simulation of machining. J Manuf Sci Eng 126(4):849–857
18. Dawson PR, Malkin S (1984) Inclined moving heat source model for calculation metal cutting temperatures. J Eng Ind 107: 179–186
19. Maekawa K, Ohhata H (1997) Simulation analysis of three-dimensional continuous chip formation processes (part 3). Int J Japan Soc Precis Eng 31(2):103–108
20. Komanduri R, Von Turkovich BF (1981) New observations on the mechanism of chip formation when machining titanium alloys. Wear 69(1):179–188
21. Komanduri R, Schroeder T, Hazra J, Von Turkovich BF, Flom DG (1982) On the catastrophic shear instability in high-speed machining of an AISI 4330 steel. J Eng Ind 104:121–131
22. Ueda N, Matsuo T (1982) An analysis of saw-toothed chip formation. Ann CIRP 31(1):81–84
23. Nakayama K, Arai M, Kanda T (1988) Machining characteristics of hard materials. Ann CIRP 37(1):89–92
24. Marusich DR, Oritz M (1995) Modelling and simulation of high speed machining. Int J Numer Meth Eng 38(21):3675–3694
25. Sandstrom DR, Hodowany JN (1998) Modeling the physics of metal cutting in high-speed machining. Mach Sci Technol 2(2): 343–353
26. Ng EG, Aspinwall DK, Brazil D, Monaghan J (1999) Modeling of temperature and forces when orthogonally machining hardened steel. Int J Mach Tools Manuf 39:885–903
27. Ng EG, Aspinwell DK (2000) Hard part machining AISI H13 ($\sim$ 50HRC) using AMBORITE AMB90: a finite element modeling approach. Ind Diamond Rev 60(587):305–310
28. Guo YB, Liu CR (2002) 3D FEA modeling of superfinish hard turning. J Manuf Sci Eng 124(2):189–199
29. Ueda T (1999) Temperature measurement of CBN tool in turning of high hardness steel. Ann CIRP 48(1):63–66
30. Hibbit, Karlson, and Sorenson, Inc. (2002) ABAQUS/Explicit user's manual, version 6.2. ABAQUS, Providence
31. Shi J, Liu CR (2004) Flow stress property of hardened steel under high temperature with tempering effect. Int J Mech Sci 46(6):891–906
32. Zener C, Hollomon JH (1944) Effect of strain rate on plastic flow of steel. J Appl Phys 14:22–32
33. MacGregor CW, Fisher JC (1945) Tension tests at constant true strain rates. J Appl Mech 15:217–227
34. Oxley PLB (1989) Mechanics of machining. Ellis Horwood, New York
35. Strenkowski JS, Carroll JT (1985) A finite element model of orthogonal metal cutting. J Eng Ind 107:349–354
36. Villars P, Prince A, Okamoto H (1995) Handbook of ternary alloy phase diagrams. ASM International, Bilthoven
37. Davies MA, Evans CJ (1996) On chip morphology, tool wear and cutting mechanics in finish hard turning. Ann CIRP 45(1):77–82
38. Orlich J (1974) The austenitization process during rapid heating and impulse heating of steel. Traitment Therm 90:69–75
39. Schrader A, Rose A (1966) Structure of steels. Stahleisen, Düsseldorf
40. Shaw MC (1998) The mechanism of chip formation with hard turning steel. Ann CIRP 47(1):77–82